Commercial vehicle-based robust control of seated whole-body vibration using adaptive indirect type-2 fuzzy neural network

Taghavifar, H., Xu, B., Hu, C., Qin, Y. & Wei, C.

DOI 10.1109/ACCESS.2020.3000514
ISSN 2169-3536

Publisher: Institute of Electrical and Electronics Engineers

IEEE Access
Multidisciplinary ⋮ Rapid Review ⋮ Open Access Journal

Received May 11, 2020, accepted May 27, 2020, date of publication June 8, 2020, date of current version July 20, 2020.

Digital Object Identifier 10.1109/ACCESS.2020.3000514

Commercial Vehicle-Based Robust Control of Seated Whole-Body Vibration Using Adaptive Indirect Type-2 Fuzzy Neural Network

HAMID TAGHAVIFAR[1], (Member, IEEE), BIN XU[2,3], CHUAN HU[4], (Member, IEEE), YECHEN QIN[2,3], (Member, IEEE), AND CHONGFENG WEI[5], (Member, IEEE)

[1]School of Mechanical, Aerospace and Automotive Engineering, Coventry University, Coventry CV1 5FB, U.K.
[2]School of Mechanical Engineering, Beijing Institute of Technology, Beijing 100081, China
[3]Beijing Institute of Technology Chongqing Innovation Center, Chongqing 401120, China
[4]Department of Mechanical Engineering, The University of Texas at Austin, Austin, TX 78712, USA
[5]Institute of Transport Studies, University of Leeds, Leeds LS2 9JT, U.K.

Corresponding author: Bin Xu (bitxubin@bit.edu.cn)

This work was supported in part by the National Science Foundation of China under Grant 51805028, and in part by the Beijing Institute of Technology Research Fund Program for Young Scholars.

ABSTRACT Drivers of commercial vehicles are invariably subject to chronic diseases such as back pain as a result of exposure to severe cabin excitations. In this paper, a six degrees of freedom (6-DOF) coupled human-body and seat suspension system is modeled in order to reduce the vibrations transmitted to the head, seat, and the relative seat and cabin floor displacement. The contributions of the present paper are: 1) two significant but inherently conflicting control objectives are employed, namely the seat acceleration and the relative displacement between seat and cabin floor to account for the effect of seat endstops, 2) A novel learning rate gradient descent based neural network approximator algorithm coupled to an adaptive indirect type-2 fuzzy neural network (T2FNN) controller to converge the controller to the ideal parameters of the uncertain model. 3) The controller model takes into account the seat suspension nonlinearities due to the nonlinear asymmetric piecewise damper and the cubic hardening of the suspension spring. The proposed controller employs the principle of type-2 fuzzy systems with interval membership function and unknown specifications. The effectiveness of the closed-loop system is validated regarding the uncertainties compared to observer-based sliding mode controller (SMC) and a high-fidelity virtual lab MSC.ADAMS-Simulink platform to validate the results in practical scenarios.

INDEX TERMS Human biodynamic model, adaptive control, seat suspension, random vibration.

I. INTRODUCTION

The prolonged occupational exposure and rough vibrations continuously exerted to the cabin are the major causes of chronic diseases, such as back pain, among the commercial vehicle drivers. Driver fatigue, discomfort, and safety have pushed the research towards improving the ride quality through the primary and secondary suspensions [1], [2]. As a remedy to this drawback, the attention has been paid to enhance the ride comfort by reducing the vibration transferred from the chassis to the driver. However, the seat suspension system is the only means of reducing the low-frequency and high-magnitude ride vibrations for a wide range of commercial vehicles. Such low-frequency and high-magnitude vibrations aggravate the ride quality when coincided with the driver's primary resonance frequency. Consequently, a generation of seat suspension systems is introduced [3], [4], which are either semi-active systems or active suspensions. However, a great body of research has focused on vibration transmission and seat control considering a rigid dummy mass on the seat which does not necessarily account for the real human body vibration [3]. Therefore, developing a mathematical model that includes the biodynamic human body is essential in order to design a control schema for the mitigation of the transmitted vibrations and to improve the safety.

The human body is optimally modeled through a high fidelity multi-degree of freedom system, the lumped mass models which involve the mass-damper-spring components can be reasonably sufficient to represent the modulus and

The associate editor coordinating the review of this manuscript and approving it for publication was Guilin Yang.

phase of the vertical seated human body characteristics exposed to random vibration in an accurate manner [5], [6]. Although there are nonlinear body models employed to investigate the effects of deformations, viscoelasticity, and nonlinear stiffness, the linearized models are suggestive of more reliable estimations depending on the validity of the model parameters [7]. There have been extensive mathematical models developed including different DOFs to capture the essential dynamics of a seated body subject to the vertically oriented vibrations [8]. The developed lumped mass models, however, typically suffer from the parametric uncertainties which arise from the subject anthropometric variations and can be drastically influenced by the mass variations.

Robust control has been the most commonly employed controller technique for seat suspension systems [9]–[12]; although fuzzy control approach has shown a reasonable capacity in the control of suspension systems [13]–[15] together with sliding mode approach [16], [17]. A combined seat-suspension model by employing 4-DOF human body model was proposed to mitigate the driver head accelerations using an H_∞ state feedback controller. The developed controller provided a smooth ride with robustness in terms of reduced driver head acceleration under typical road disturbances [18]. Lathkar *et al.* [19] developed an active seat suspension system with robustness to uncertainties and external disturbances by incorporating the observer for the state and disturbance using sliding mode control scheme. The designed controller operated based on the seat position measurement while a 4-DOF biodynamic model of the seated body was employed for the analysis of developed controller. The designed model, however, was a simplified linear system tested on a relatively smooth road surface (ISO class C), which does not typically impose high-frequency or high-amplitude excitations. Furthermore, the control input generated high-frequency component signals due to the chattering phenomenon. Similarly, a terminal sliding mode controller including the disturbance observer and state observer was developed for the seat suspension control through an integrated 6DOF seat and driver model [20]. Linear Matrix Inequality (LMI) technique was also employed for the disturbance and state observers while a filter was designed in order to achieve an enhanced observer performance. However, such controllers could potentially fail to reach the actual optimal performance and thereby it is essential to further investigate the issues related to the improved performance of sliding mode control (SMC) and ensure the robustness for nonlinear active suspension systems [21]. Ning *et al.* [22], proposed a two-layer multiple-DOF seat suspension including a bottom-layer suspension for vertical vibration control and a top-layer suspension with two independently controlled rotational DOFs. Their approach is suggestive of the advantage of independently controlling the vertical and fore-aft vibrations but at the cost of further employing more than three actuators and thereby a significant power demand. Furthermore, the employed SMC control method may bring about chattering and singularity problems. This is in addition to the major drawback of SMC which is its failure to provide a nominal optimal performance for active suspension system because the efficiency of these robust control schemes for the seat suspension control can be reduced [21].

Fuzzy-neural network (FNN) systems have shown a great capacity to deal with modeling and control of the complex and nonlinear processes at a reasonably acceptable degree of accuracy by employing the universal approximation capacity [23], [24]. The primary advantage of fuzzy Takagi-Sugeno based systems is the use of a set of local linear systems through the associated membership functions that can handle the nonlinear functions. The estimation procedure for any nonlinear system may thus be performed satisfactorily. The convergence of the error towards a small neighborhood of origin and the bounded outputs are the major limitations of the adaptive fuzzy control technique through output-feedback when employed for the nonlinear and uncertain systems [25], [26]. However, type-2 fuzzy systems exhibit an enhanced efficiency when compared to the type-1 systems exposed to structured and unstructured uncertainties [27], [28], mainly because the membership functions are also described in a fuzzy manner. A type-2 fuzzy system is defined by if-then rules while the antecedent or consequent sets are also type-2 [29]. The adaptive fuzzy controllers can be considered either as a direct or indirect method wherein the later employs the fuzzy explanations to model the system rather than directly employing the linguistic rules.

The reviewed literature reveals the following issues. The robust control strategy is a commonly employed technique for the seat suspension control owing to the considerable parametric uncertainties related to the gender and anthropometric variability and the presence of external disturbances. The commonly employed H∞ and SMC methods either suffer from the failure to reach an actual optimal performance and chattering and singularity problems. However, fuzzy type-2 can serve as a decent robust controller method to address the uncertainty and external disturbances. Furthermore, most of the studies in the literature have not considered the cabin excitations for rough condition or through standardized methods (ISO 7096) [31] and consideration of the weighted acceleration of the human body (ISO 2631) [32] through the filter design which underestimates the true transmitted accelerations to the driver body. Finally, a novel learning rate gradient descent-based neural network approximator algorithm coupled to an adaptive indirect type-2 fuzzy neural network (T2FNN) controller is employed for the asymptotic convergence of the system states.

The rest of the paper is organized as follows. Section *II* formulates the problem and the required filters are designed and modeled, transmissibility functions and PSD analysis formulations are presented for the analysis in the frequency domain. Section *III* and *IV* are dedicated to the description of the fuzzy type-2 neural network system and the design of the proposed controller, respectively. The model is implemented by employing a high-fidelity and virtual lab MSC.ADAMS platform for the validation of the proposed controller for

practical implementations. In section *V*, the results are presented and discussed and finally, section *VI* concludes the paper.

II. PROBLEM STATEMENT

The vertically oriented motions of the seat suspension and human body segments are shown in Fig. 1 while the pitch and roll motions of the body are ignored due to the negligible contribution of these modes. The driver lumped mass model includes different segments of the body. Furthermore, the effect of road excitations on the seat frame is modeled using a designed filter according to ISO 7096. Therefore, a controller is proposed to mitigate the vibrations transferred through the seat to the driver body. As can be appreciated from Fig. 1, the human body is represented by four major segments and the remaining parts are those of seat cushion and seat frame. The coupled human-seat lumped mass model parameters together with the nonlinear seat suspension components are presented in Table 1. The human biodynamic model through the lumped mass system was obtained from series of experimental tests on human subjects [33]. The procedure completed by an optimization process applied to the human body biodynamic testing data as the constraints, and minimization of the error between the seat-to-head transmissibility, driving-point mechanical impedance, and apparent mass data. It is noteworthy that the role of lower legs and feet has been ignored owing to the insignificant contributions to the human body model and the effect of the arms is combined with the upper torso. In the schematic model, $\{z_1, \ldots, z_6\}$ denote the displacements of different parts, z_0 is the cabin excitation, and u is the active control input of the seat suspension system, respectively. The seat cushion is represented through a set of springs and dampers elements whose characteristics are constant. The governing mathematical model

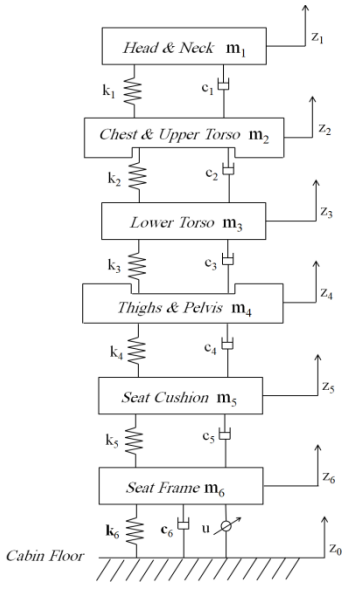

FIGURE 1. The coupled 6DOF human-body and seat suspension model.

TABLE 1. The coupled human-seat lumped mass model parameters.

Mass (kg)		Damping coefficient (Ns/m)		Spring stiffness (N/m)	
m_1	5.31	c_1	400	k_1	310000
m_2	28.49	c_2	4750	k_2	183000
m_3	8.62	c_3	4585	k_3	162800
m_4	12.78	c_4	2064	k_4	90000
m_5	1	c_5	200	k_5	18000
m_6	15	c_{6e1}	4830	k_{6l}	29997
		c_{6e2}	6130	k_{6nl}	85000
		c_{6c1}	2450		
		c_{6c2}	2500		

* v_e and v_c are considered at 0.1156 m/s and 0.1164 m/s, respectively.

describing the multi-segment driver model and the nonlinear seat suspension system using a cubic hardening stiffness and the nonlinear asymmetric piecewise damper is developed as follows.

$$\ddot{z}_1 = -\omega_{n1}^2 (z_1 - z_2) - 2\zeta_1\omega_{n1} (\dot{z}_1 - \dot{z}_2) \tag{1}$$

$$\ddot{z}_2 = \vartheta_{m1}\omega_{n1}^2 (z_1 - z_2) + 2\vartheta_{m1}\zeta_1\omega_{n1} (\dot{z}_1 - \dot{z}_2) - \omega_{n2}^2 (z_2 - z_3) - 2\zeta_2\omega_{n2} (\dot{z}_2 - \dot{z}_3) \tag{2}$$

$$\ddot{z}_3 = \vartheta_{m2}\omega_{n2}^2 (z_2 - z_3) + 2\vartheta_{m2}\zeta_2\omega_{n2} (\dot{z}_2 - \dot{z}_3) - \omega_{n3}^2 (z_3 - z_4) - 2\zeta_3\omega_{n3} (\dot{z}_3 - \dot{z}_4) \tag{3}$$

$$\ddot{z}_4 = \vartheta_{m3}\omega_{n3}^2 (z_3 - z_4) + 2\vartheta_{m3}\zeta_3\omega_{n3} (\dot{z}_3 - \dot{z}_4) - \omega_{n4}^2 (z_4 - z_5) - 2\zeta_4\omega_{n4} (\dot{z}_4 - \dot{z}_5) \tag{4}$$

$$\ddot{z}_5 = \vartheta_{m4}\omega_{n4}^2 (z_4 - z_5) + 2\vartheta_{m4}\zeta_4\omega_{n4} (\dot{z}_4 - \dot{z}_5) - \omega_{n5}^2 (z_5 - z_6) - 2\zeta_5\omega_{n5} (\dot{z}_5 - \dot{z}_6) \tag{5}$$

$$\ddot{z}_6 = \vartheta_{m5}\omega_{n5}^2 (z_5 - z_6) + 2\vartheta_{m5}\zeta_5\omega_{n5} (\dot{z}_5 - \dot{z}_6) - \frac{1}{m_6}\left[k_{6l} (z_6 - z_0) - k_{6nl} (z_6 - z_0)^3 - F_d - u\right] \tag{6}$$

$$\omega_{ni}^2 = \frac{k_i}{m_i}, \quad \zeta_i = \frac{c_i}{2\sqrt{k_i m_i}}, \quad \vartheta_{mi} = \frac{m_i}{m_{i+1}}, \quad i = 1, 2 \ldots, 5 \tag{7}$$

where ω_{ni}, ζ_i and ϑ_{mi} denote the natural frequencies, damping ratio and mass ratio, respectively. Furthermore, the nonlinear asymmetric piecewise damping force generated by the dampers are presented as follows.

$$F_d = \begin{cases} c_{6e1} (\dot{z}_6 - \dot{z}_0) & v_e \leq \dot{z}_6 - \dot{z}_0 < 0 \\ c_{6e1} v_e + c_{6e2} (\dot{z}_6 - \dot{z}_0) & \dot{z}_6 - \dot{z}_0 < v_e \\ c_{6c1} (\dot{z}_6 - \dot{z}_0) & 0 \leq \dot{z}_6 - \dot{z}_0 < v_c \\ c_{6c1} v_c + c_{6c2} (\dot{z}_6 - \dot{z}_0) & v_c < \dot{z}_6 - \dot{z}_0 \end{cases} \tag{8}$$

where c_{6c2}, c_{6e2}, c_{6c1} and c_{6e1} represent the low and high damping coefficients in the compression and rebound modes, respectively with the corresponding transition velocities v_c and v_e. The governing equations developed from (1) to (6) can be rewritten in terms of the complex transmissibility functions in order to describe the power spectral density (PSD) of the transmitted vibration to different body segments in the frequency domain. The transfer functions from the seat (z_6) to any of the body segments could be determined by solving the Laplace domain functions. The transfer functions from

the seat to the Thighs and Pelvis ($T_{z_6}^{z_4}$) and to the head ($T_{z_6}^{z_1}$) are obtained as follows.

$$\begin{aligned} T_{z_6}^{z_4}(s) &= \frac{Z_4(s)}{Z_6(s)} = E(s)G(s) \\ T_{z_6}^{z_1}(s) &= \frac{Z_1(s)}{Z_6(s)} = A(s)B(s)D(s)E(s)G(s) \\ T_{z_0}^{z_5-z_6}(s) &= \frac{Z_5(s)-Z_6(s)}{Z_6(s)} = E(s)g(s)-1 \end{aligned} \tag{9}$$

where, $Z_5(s)$, $Z_4(s)$, $Z_1(s)$, and $Z_0(s)$ represent the Laplace transforms of $z_5(t)z_4(t)$, $z_1(t)$, and $z_0(t)$, and the remaining Laplace functions are described by

$$\begin{aligned} A(s) &= \frac{\omega_{n1}^2 + 2s\zeta_1\omega_{n1}}{s^2+\omega_{n1}^2+2s\zeta_1\omega_{n1}} \\ B(s) &= \frac{\omega_{n2}^2 + 2s\zeta_2\omega_{n2}}{s^2+\omega_{n2}^2+2s\zeta_2\omega_{n2}+\vartheta_{m1}\left(\omega_{n1}^2+2s\zeta_1\omega_{n1}\right)+A(s)} \\ D(s) &= \frac{\omega_{n3}^2 + 2s\zeta_3\omega_{n3}}{s^2+\omega_{n3}^2+2s\zeta_3\omega_{n3}+\vartheta_{m2}\left(\omega_{n2}^2+2s\zeta_2\omega_{n2}\right)+B(s)} \\ E(s) &= \frac{\omega_{n4}^2 + 2s\zeta_4\omega_{n4}}{s^2+\omega_{n4}^2+2s\zeta_4\omega_{n4}+\vartheta_{m3}\left(\omega_{n3}^2+2s\zeta_3\omega_{n3}\right)+D(s)} \\ G(s) &= \frac{\omega_{n5}^2 + 2s\zeta_5\omega_{n5}}{s^2+\omega_{n5}^2+2s\zeta_5\omega_{n5}+\vartheta_{m4}\left(\omega_{n4}^2+2s\zeta_4\omega_{n4}\right)+E(s)} \end{aligned} \tag{10}$$

where s denotes the Laplace parameter and may be substituted by $j\omega$ where $j=\sqrt{-1}$ in order to describe the functions in the frequency domain. Considering the seat PSD, $S_{\ddot{z}_6}(\omega)$, and based on the transfer functions to the head, $T_{z_6}^{z_1}(\omega)$, and seat acceleration which is related to the force exerted to the driver at the seat interface $T_{z_6}^{z_4}(\omega)$, and the relative seat displacement, $T_{\ddot{z}_6}^{\delta_{z_5-z_6}}(\omega)$, PSD functions related to each of these modes can be formulated by:

$$\begin{aligned} S_{\ddot{z}_1}(\omega) &= \left|T_{z_6}^{z_1}(\omega)\right|^2 S_{\ddot{z}_6}(\omega) \\ S_{\ddot{z}_4}(\omega) &= \left|T_{z_6}^{z_4}(\omega)\right|^2 S_{\ddot{z}_6}(\omega) \\ S_{\delta_{z_5-z_6}}(\omega) &= \left|T_{\ddot{z}_0}^{\delta_{z_5-z_6}}(\omega)\right|^2 S_{\ddot{z}_6}(\omega) \\ &= \left[\left|T_{z_6}^{\delta_{z_5-z_6}}(\omega)-1\right|^2 / \omega^4\right] S_{\ddot{z}_6}(\omega) \end{aligned} \tag{11}$$

By introducing the above PSD functions, the root mean square (RMS) accelerations at the seat, head and the relative seat displacement can be derived through the following functions:

$$\begin{aligned} \sigma_{\ddot{z}_1} &= \sqrt{\int_0^\infty S_{\ddot{z}_1}(\omega)\,d\omega}, \quad \sigma_{\ddot{z}_4} = \sqrt{\int_0^\infty S_{\ddot{z}_4}(\omega)\,d\omega}, \\ \sigma_{\delta_{z_5-z_6}} &= \sqrt{\int_0^\infty S_{\delta_{z_5-z_6}}(\omega)\,d\omega} \end{aligned} \tag{12}$$

However, one should note that the calculated acceleration terms are those obtained from the weighted accelerations obtained from the filter design, where the total weighting function is represented as follows

$$H(\tilde{\rho}) = H_h(\tilde{\rho}).H_l(\tilde{\rho}).H_t(\tilde{\rho}).H_s(\tilde{\rho}) \tag{13}$$

where $\tilde{\rho}=j2\pi\rho$ is the imaginary angular frequency, and the complex function is described in the frequency domain where the modulus and phase can be determined. Furthermore, the product term $H_h(\tilde{\rho}).H_l(\tilde{\rho})$ represents the band-limiting transfer function and the product term $H_t(\tilde{\rho}).H_s(\tilde{\rho})$ denotes the actual weighting transfer function indicated by infinity frequencies.

The modulus of the transfer functions can be further described. The band-limiting two-pole filter with Butterworth characteristics can be presented in terms of a high-pass and low-pass functions as follows:

$$|H_h(\tilde{\rho})| = \left|\frac{\tilde{\rho}^2}{\tilde{\rho}^2+\sqrt{2}\tilde{\rho}\omega_1+\omega_1^2}\right| \tag{14}$$

and the low-pass term is represented by:

$$|H_l(\tilde{\rho})| = \left|\frac{\tilde{\rho}^2}{\tilde{\rho}^2+\sqrt{2}\tilde{\rho}\omega_2+\omega_2^2}\right| \tag{15}$$

where $\omega_1 = 2\pi f_1$, $\omega_2 = 2\pi f_2$ and f_1 and f_2 are the corner frequencies at 0.4 and 100 Hz, respectively. Furthermore, the acceleration to velocity transition which is related to acceleration at lower frequencies and relative to the velocity at higher frequencies can be calculated from

$$|H_t(\tilde{\rho})| = \left|\frac{Q_4\omega_4^2\left[\tilde{\rho}+\omega_3\right]}{\omega_3\left[Q_4\tilde{\rho}^2+\tilde{\rho}\omega_4+Q_4\omega_4^2\right]}\right| \tag{16}$$

where $\omega_3 = 2\pi f_3, \omega_4 = 2\pi f_4$ and f_3 and f_4 are the frequencies both at 12.5 Hz, and Q_4 is the parameter of the transfer function related to the overall frequency weighting and is typically 0.63, respectively. Finally, the upward step which is the steepness about 6 dB per octave and related to jerk and can be described as

$$|H_s(\tilde{\rho})| = \left|\frac{Q_6\left[Q_5\tilde{\rho}^2+\tilde{\rho}\omega_5+Q_5\omega_5^2\right]}{Q_5\left[Q_6\tilde{\rho}^2+\tilde{\rho}\omega_6+Q_6\omega_6^2\right]}\right| \tag{17}$$

where $\omega_5 = 2\pi f_5$, $\omega_6 = 2\pi f_6$ and f_5 and f_6 are the frequencies at 2.37 and 3.35, respectively, and Q_5 and Q_6 are the parameters of the transfer function at 0.91, respectively. The filter design for the cabin excitations are also presented for a typical soil compacter commercial vehicle (EM5, ISO 7096) as follows based on the input spectral

$$EM5 = 1.11\,(HP24)^2\,(LP6)^2 \tag{18}$$

where HP and LP designate the high-pass and low-pass filters of the Butterworth type defined in (19) and the subordinated numbers are the filter slopes in decibels per octave.

$$\begin{aligned} LP6 &= \frac{1}{S+1} \\ HP24 &= \frac{S^4}{S^4+2.613S^3+3.414S^2+2.613S+1} \end{aligned} \tag{19}$$

where $S = j\rho/f_c$ and f_c is the filter cut-off frequency. The further details of the developed filter in term of the cut-off frequencies and the PSD magnitude will be further mentioned in the results and discussion section.

III. INTERVAL TYPE-2 FUZZY LOGIC SYSTEM

Assume the equations of motion can be written in the state-space form in (20) $\left(\begin{matrix} \dot{x}_i = z_i \\ \dot{z}_j = \dot{z}_i \end{matrix} i = 1, 2, \ldots 6; j = 7, 8, \ldots 12\right)$

$$\dot{x}_1 = x_7, \quad \dot{x}_2 = x_8, \; \dot{x}_3 = x_9, \; \dot{x}_4 = x_{10}, \; \dot{x}_5 = x_{11},$$
$$\dot{x}_6 = x_{12} \tag{20a}$$
$$\dot{x}_7 = -\omega_{n1}^2 (x_1 - x_2) - 2\zeta_1\omega_{n1} (x_7 - x_8) \tag{20b}$$
$$\dot{x}_8 = \vartheta_{m1}\omega_{n1}^2 (x_1 - x_2) + 2\vartheta_{m1}\zeta_1\omega_{n1} (x_7 - x_8) - \omega_{n2}^2 (x_2 - x_3) - 2\zeta_2\omega_{n2} (x_8 - x_9) \tag{20c}$$
$$\dot{x}_9 = \vartheta_{m2}\omega_{n2}^2 (x_2 - x_3) + 2\vartheta_{m2}\zeta_2\omega_{n2} (x_8 - x_9) - \omega_{n3}^2 (x_3 - x_4) - 2\zeta_3\omega_{n3} (x_9 - x_{10}) \tag{20d}$$
$$\dot{x}_{10} = \vartheta_{m3}\omega_{n3}^2 (x_3 - x_4) + 2\vartheta_{m3}\zeta_3\omega_{n3} (x_9 - x_{10}) - \omega_{n4}^2 (x_4 - x_5) - 2\zeta_4\omega_{n4} (x_{10} - x_{11}) \tag{20e}$$
$$\dot{x}_{11} = \vartheta_{m4}\omega_{n4}^2 (x_4 - x_5) + 2\vartheta_{m4}\zeta_4\omega_{n4} (x_{10} - x_{11}) - \omega_{n5}^2 (x_5 - x_6) - 2\zeta_5\omega_{n5} (x_{11} - x_{12}) \tag{20f}$$
$$\dot{x}_{12} = \vartheta_{m5}\omega_{n5}^2 (x_5 - x_6) + 2\vartheta_{m5}\zeta_5\omega_{n5} (x_{11} - x_{12}) - \frac{1}{m_6}\left[k_{6l} (x_6 - z_0) - k_{6nl} (x_6 - z_0)^3 - F_d - u\right] \tag{20g}$$
$$F_d = \begin{cases} c_{6e1} (x_{12} - \dot{z}_0) & v_e \le x_{12} - \dot{z}_0 < 0 \\ c_{6e1} v_e + c_{6e2} (x_{12} - \dot{z}_0) & x_{12} - \dot{z}_0 < v_e \\ c_{6c1} (x_{12} - \dot{z}_0) & 0 \le x_{12} - \dot{z}_0 < v_c \\ c_{6c1} v_c + c_{6c2} (x_{12} - \dot{z}_0) & v_c < x_{12} - \dot{z}_0 \end{cases} \tag{20h}$$
$$\dot{\boldsymbol{x}} = \boldsymbol{f}(\boldsymbol{x}) + \boldsymbol{g}(\boldsymbol{x})\, u + \boldsymbol{d}(z) \tag{21}$$

where $\boldsymbol{x} = [x_1, x_2 \ldots, x_{12}]^T$, $\boldsymbol{z} = [z_0, \dot{z}_0]$ $\boldsymbol{f}(.)$ and $\boldsymbol{g}(.)$ are uncertain but bounded functions, $u(t) \in R$, and $\boldsymbol{d}(.)$ is the disturbance due to the excitations at the cabin floor, according to (20). The primary objective of the designed controller is to attenuate the vibrations transferred to the chassis and the driver's head. A standard fuzzy type-2 interval-based membership function characterized by mean μ is shown in Figure 2. Furthermore, σ_1 and σ_2 indicate the unknowns

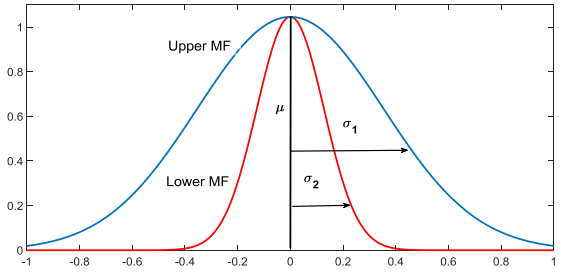

FIGURE 2. Representation of a standard interval-based fuzzy type-2 fuzzy membership function.

standard deviations corresponding to the upper and lower membership functions. These parameters are updated through the controller design procedure and the architecture of the employed T2FNN and the proposed controller body diagram are illustrated in Fig. 3.

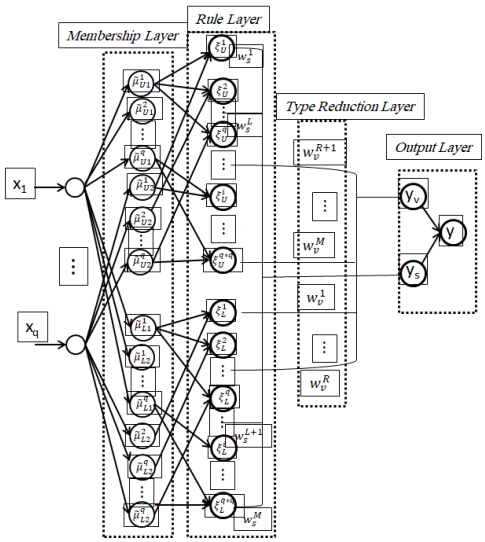

FIGURE 3. Architecture of the proposed T2FNN structure.

The concept of interval-based fuzzy type-2 system is discussed herein as well as the inference logic mechanism. Commonly speaking, a system that contains at least one fuzzy type-2 membership function is regarded as a type-2 fuzzy logic system [17], [29]. In such a system, the interval type-2 fuzzy set $\tilde{A}$ within domain X is expressed as [30]

$$\tilde{A} = \int_{x \in X} \frac{\left[\int_{\tilde{u} \in J_x} \tilde{u}^{-1}\right]}{x} \qquad J_x \subseteq [0\ 1] \tag{22}$$

where J_x represents the trace of the corresponding fuzzy set variations, x and $\tilde{u}$ hold the main and dependent variables described in the region X. In general, computation of the type-2 fuzzy system for M rules and q inputs is described in the form of

$$\begin{aligned} \text{Rule}^{\text{i}}: \quad & \text{IF } x_1 \text{ is } \tilde{A}_1^i \text{ and } x_2 \text{ is } \tilde{A}_2^i \ldots x_q \text{ is } \tilde{A}_1^i \\ & \text{THEN } y \text{ is } \underline{y}^i \quad i = 1, 2, \ldots, M \end{aligned} \tag{23}$$

The primary variable in the input vector and thereby, $\boldsymbol{x} = (x_1, x_2, \ldots, x_q)$ and y are descendant linguistic variables, $\tilde{A}_q^i$ denote the fuzzy type-2 set where $q = 1, 2, \ldots, 12$ and $\underline{y}^i = [y_v^i, y_s^i]$, as shown in Fig. 3.

The data for the selected fuzzy system herein is briefly mentioned as:

1: The unprocessed data are supplied to the system in the first layer in the form of some inputs.

2: The specifications of the interval-based fuzzy membership functions are set in the second layer. Additionally, the outputs of the system are taken, each attributed to a

range of membership in terms of the connecting nods. These nods convey a particular average value μ yet undetermined standard deviations σ_1 and σ_2. The mean values for each of the upper and lower functions are described as:

$$\begin{aligned}\overline{\mu}_i^q(x_q) &= exp\left(-\frac{1}{2}\left(\frac{x_q-\mu_i^q}{\overline{\sigma}_i^q}\right)^2\right)\\ \underline{\mu}_i^q(x_q) &= exp\left(-\frac{1}{2}\left(\frac{x_q-\mu_i^q}{\underline{\sigma}_i^q}\right)^2\right)\end{aligned} \tag{24}$$

where $\overline{\mu}_i^q(x_q)$ and $\underline{\mu}_i^q(x_q)$ symbolize the higher and lower varieties of the firing limits related to the outputs of i^{th} higher and lower membership functions, respectively and the q^{th} input [29]. Furthermore, μ_i^q represents the average and $\sigma = \left[\overline{\sigma}_i^q.\underline{\sigma}_i^q\right]$ denotes the undetermined amplitude of i^{th} higher and lower membership functions related to the q^{th} input, respectively [29].

3: The output from layer 2 is taken here as the input of the third layer where the multiplication is applied to the inputs. The main purpose of this layer is to determine the power of the upper and lower firing rules [17]. Therefore, the nodes are related to the rules where entire of M rules are accessible for any of the higher and lower functions as:

$$\begin{aligned}\bar{\chi}^i(x) &= \overline{\mu}_{\tilde{A}_1^i}(x_1)\times\overline{\mu}_{\tilde{A}_2^i}(x_2)\times\ldots\overline{\mu}_{\tilde{A}_q^i}(x_q)\\ \underline{\chi}^i(x) &= \underline{\mu}_{\tilde{A}_1^i}(x_1)\times\underline{\mu}_{\tilde{A}_2^i}(x_2)\times\ldots\underline{\mu}_{\tilde{A}_q^i}(x_q)\end{aligned} \tag{25}$$

where $\overline{\mu}_{\tilde{A}_1^i}$ and $\underline{\mu}_{\tilde{A}_1^i}$ are the i^{th} upper and lower degrees of membership, respectively.

4: The variables s and w are used in this layer for the type reduction purpose according to the center of sets concept [17], in which the results denoted by y_S and y_v are derived in compliance with [34]. The defuzzified centers of the fuzzy sets require that each rule consequent to be defined by a singleton positioned at the center [29]. The Karnek-Mendel-Liang iterative technique [35] defines the output according to:

$$\begin{aligned}y_s &= \frac{\sum_{i=1}^{L}\underline{\chi}^i w_s^i+\sum_{i=L+1}^{M}\bar{\chi}^i w_s^i}{\sum_{i=1}^{L}\underline{\chi}^i+\sum_{i=1}^{M}\bar{\chi}^i}\\ y_v &= \frac{\sum_{i=1}^{R}\underline{\chi}^i w_v^i+\sum_{i=R+1}^{M}\bar{\chi}^i w_v^i}{\sum_{i=1}^{R}\underline{\chi}^i+\sum_{i=1}^{M}\bar{\chi}^i}\end{aligned} \tag{26}$$

where w_v^i and w_s^i represent the sequential variables in the i^{th} rules related to the higher and lower firing rules. Additionally, R and L are obtained according to the Karni–Mendel technique [35]. Considering those of M rules for the upper and lower MFs, w_v^i and w_s^i represent the weighting factors concerned with y_s and y_v being defined as:

$$\begin{aligned}w_v^i &= \alpha_{q-1}^i+\alpha_q^i x_j+\alpha_{q+1}^i x_{q+1}\ldots\\ w_s^i &= \beta_{j-1}^i+\beta_j^i x_j+\beta_{j+1}^i x_{j+1}+\ldots\\ i &= 1,2,\ldots,M;\quad q=1,2,\ldots,12\end{aligned} \tag{27}$$

where x_q represents the signals sent to fuzzy system, q defines the input size, and α_j^i and β_j^i determine the adaptive variables related to the i^{th} MF and $\tilde{j}^{th}$ updated inputs. By assuming

$$\begin{aligned}\delta_s &= \sum_{i=1}^{L}\underline{\chi}^i+\sum_{i=1}^{M}\bar{\chi}^i,\\ \delta_v &= \sum_{i=1}^{R}\underline{\chi}^i+\sum_{i=1}^{M}\bar{\chi}^i,\\ \underline{Q}_s^i &= \underline{\chi}^i/\delta_s,\quad \overline{Q}_s^i=\bar{\chi}^i/\delta_s,\ \underline{Q}_v^i=\underline{\chi}^i/\delta_v,\end{aligned}$$

and

$$\overline{Q}_v^i = \bar{\chi}^i/\delta_v, \tag{28}$$

can be considered as

$$\begin{aligned}y_s &= \sum_{i=1}^{L}\underline{Q}_s^i w_s^i+\sum_{i=L+1}^{M}\overline{Q}_s^i w_s^i=\Theta_s^T\xi_s\\ y_v &= \sum_{i=1}^{L}\underline{Q}_v^i w_v^i+\sum_{i=L+1}^{M}\overline{Q}_v^i w_v^i=\Theta_v^T\xi_v\end{aligned} \tag{29}$$

where $\xi_s^T = \left[\underline{Q}_s^i,\overline{Q}_s^i\right]$, $\Theta_s^T = \left[\underline{w}_s^i,\overline{w}_s^i\right]$, $\xi_v^T = \left[\underline{Q}_v^i,\overline{Q}_v^i\right]$, and $\Theta_v^T = \left[\underline{w}_v^i,\overline{w}_v^i\right]$.

5: Lastly, the outputs are derived in this layer based on an averaging rule obtained from (29) as perceived from Fig. 3.

$$y = \frac{(y_s+y_v)}{2} \tag{30}$$

IV. PROPOSED CONTROL LAW

It is possible to predict the unknown functions of $f(x)$ and $g(x)$ in (20) through a developed T2FNN, while $\tilde{f}\left(x|\Theta_f^*\right)$ and $\tilde{g}\left(x|\Theta_g^*\right)$ are the ideal estimations of the unknown functions. Furthermore, Ω represents a compact domain that contains the extent of x, and Θ_f and Θ_g hold the parameters that are adjusted and updated through the training procedure (μ, σ_1, σ_2, w_v^i and w_s^i).

$$\begin{aligned}\Theta_f^* &:= \arg\min_{\Theta_f\in\mathbb{R}^{\prod_{i=1}^{n}p_i}}\left\{\sup_{x\in\Omega}\left|\tilde{f}\left(x|\Theta_f\right)-f(x)\right|\right\}\\ \Theta_g^* &:= \arg\min_{\Theta_g\in\mathbb{R}^{\prod_{i=1}^{n}q_i}}\left\{\sup_{x\in\Omega}\left|\tilde{g}\left(x|\Theta_g\right)-g(x)\right|\right\}\end{aligned} \tag{31}$$

And the functions above can be further described by the developed Taylor's expansion about the points of the unknown functions:

$$\begin{aligned}\tilde{f}\left(\boldsymbol{x}|\boldsymbol{\Theta}_f^*\right)-\tilde{f}\left(\boldsymbol{x}|\boldsymbol{\Theta}_f\right) &= \left(\boldsymbol{\Theta}_f^*-\boldsymbol{\Theta}_f\right)^T\left[\frac{\partial\tilde{f}\left(\boldsymbol{x}|\boldsymbol{\Theta}_f\right)}{\partial\boldsymbol{\Theta}_f}\right]\\ &\quad+h.o.t\left(\left|\boldsymbol{\Theta}_f^*-\boldsymbol{\Theta}_f\right|^2\right)\\ \tilde{g}\left(\boldsymbol{x}|\boldsymbol{\Theta}_g^*\right)-\tilde{g}\left(\boldsymbol{x}|\boldsymbol{\Theta}_g\right) &= \left(\boldsymbol{\Theta}_g^*-\boldsymbol{\Theta}_g\right)^T\left[\frac{\partial\tilde{g}\left(\boldsymbol{x}|\boldsymbol{\Theta}_g\right)}{\partial\boldsymbol{\Theta}_g}\right]\\ &\quad+h.o.t\left(\left|\boldsymbol{\Theta}_g^*-\boldsymbol{\Theta}_g\right|^2\right)\end{aligned} \tag{32}$$

where $h.o.t\left(\left|\boldsymbol{\Theta}_f^*-\boldsymbol{\Theta}_f\right|^2\right)$ and $h.o.t\left(\left|\boldsymbol{\Theta}_g^*-\boldsymbol{\Theta}_g\right|^2\right)$ describe the higher order terms of any of the expressions, respectively. Therefore, the estimated $\tilde{\boldsymbol{f}}\left(\boldsymbol{x}|\boldsymbol{\Theta}_f\right)$ and $\tilde{\boldsymbol{g}}\left(\boldsymbol{x}|\boldsymbol{\Theta}_f\right)$ can be considered an alternative for the ideal estimated functions $\tilde{\boldsymbol{f}}\left(\boldsymbol{x}|\boldsymbol{\Theta}_f^*\right)$ and $\tilde{\boldsymbol{g}}\left(\boldsymbol{x}|\boldsymbol{\Theta}_g^*\right)$:

$$\begin{aligned}\tilde{\boldsymbol{f}}\left(\boldsymbol{x}|\boldsymbol{\Theta}_f\right) &= \boldsymbol{\Theta}_f^T\boldsymbol{\xi}_f\left(\boldsymbol{x}\right)+\boldsymbol{\varepsilon}_f(\boldsymbol{x})\\ \tilde{\boldsymbol{g}}\left(\boldsymbol{x}|\boldsymbol{\Theta}_g\right) &= \boldsymbol{\Theta}_g^T\boldsymbol{\xi}_g\left(\boldsymbol{x}\right)+\boldsymbol{\varepsilon}_g(\boldsymbol{x})\end{aligned} \tag{33}$$

where

$$\begin{aligned}\boldsymbol{\xi}_f &= \frac{\partial\tilde{\boldsymbol{f}}\left(\boldsymbol{x}|\boldsymbol{\Theta}_f\right)}{\partial\boldsymbol{\Theta}_f}\\ \boldsymbol{\xi}_g &= \frac{\partial\tilde{\boldsymbol{g}}\left(\boldsymbol{x}|\boldsymbol{\Theta}_g\right)}{\partial\boldsymbol{\Theta}_g}\end{aligned} \tag{34}$$

The estimated functions $\boldsymbol{\Theta}_f^T\boldsymbol{\xi}_f(\boldsymbol{x})$ and $\boldsymbol{\Theta}_g^T\boldsymbol{\xi}_g(\boldsymbol{x})$ bring about the tracking errors $\boldsymbol{\varepsilon_f}(\boldsymbol{x})$ and $\boldsymbol{\varepsilon_g}(\boldsymbol{x})$. Additionally, $\boldsymbol{\theta_f}=\left[\Theta_{f1},\Theta_{f2},\ldots,\Theta_{fn}\right]$ and $\boldsymbol{\theta_g}=\left[\Theta_{g1},\Theta_{g2},\ldots,\Theta_{gn}\right]$ are the vectors of tuning parameters and $\boldsymbol{\xi_f}(\boldsymbol{x})=\left[\xi_{f1}(\boldsymbol{x}),\xi_{f2}(\boldsymbol{x}),\ldots,\xi_{fn}(\boldsymbol{x})\right]$ and $\boldsymbol{\xi_g}(\boldsymbol{x})=\left[\xi_{g1}(\boldsymbol{x}),\xi_{g2}(\boldsymbol{x}),\ldots,\xi_{gn}(\boldsymbol{x})\right]$ are the T2FNN vectors and $\boldsymbol{\varepsilon_f}(\boldsymbol{x})$ and $\boldsymbol{\varepsilon_g}(\boldsymbol{x})$ are the estimation error subject to minimization of (31). We make the following assumption that on a compact region $\Omega\in R$:

$$|\boldsymbol{\varepsilon}(\boldsymbol{x})|\le\lambda\quad\forall\boldsymbol{x}\in\mathbb{R} \tag{35}$$

where $\lambda\ge 0$ is an unknown bound which is the smallest non-negative constant to satisfy (29). If functions of $\boldsymbol{f}(\boldsymbol{x})$ and $\boldsymbol{g}(\boldsymbol{x})$ were known or obtained through an approximator, the ideal control law can be described through the feedback linearization theory as follows

$$u_*=\frac{\left[-\boldsymbol{f}(\boldsymbol{x})+\boldsymbol{y}_m^{(n)}+\boldsymbol{K}^T\boldsymbol{e}\right]}{\boldsymbol{g}(\boldsymbol{x})+\boldsymbol{\alpha}} \tag{36}$$

where $\boldsymbol{\alpha}$ denotes compensator to deal with the function (30) singularity issue. By substituting the (30) in (21), the dynamics of the tracking error, $\boldsymbol{e}$, can be obtained as:

$$\boldsymbol{e}^{(n)}+k_1\boldsymbol{e}^{(n-1)}+\ldots+k_n\boldsymbol{e}=0 \tag{37}$$

where $\boldsymbol{K}=[k1,k1,\ldots kn]^T$ are selected such that the polynomial (37) is Hurwitz stable. However, as the functions are unknown, thereby (36) can be presented in terms of the estimated functions:

$$u_*=\left[\tilde{\boldsymbol{g}}(\boldsymbol{x})+\boldsymbol{\alpha}\right]^{-1}\left[-\tilde{\boldsymbol{f}}(\boldsymbol{x})+\boldsymbol{y}_m^{(n)}+\boldsymbol{K}^T\boldsymbol{e}\right] \tag{38}$$

Substituting (38) in (21), the following dynamics of the tracking error is achieved

$$\boldsymbol{e}^{(n)}=-\boldsymbol{K}^T\boldsymbol{e}+\left[\tilde{\boldsymbol{f}}(\boldsymbol{x})-\boldsymbol{f}(\boldsymbol{x})\right]+\left[\tilde{\boldsymbol{g}}(\boldsymbol{x})-\boldsymbol{g}(\boldsymbol{x})\right]u_* \tag{39}$$

In this manner, the optimal approximation error is considered to be

$$\tilde{\boldsymbol{w}}=\left[\tilde{\boldsymbol{f}}\left(\boldsymbol{x}|\boldsymbol{\Theta}_f^*\right)-\boldsymbol{f}(\boldsymbol{x})\right]+\left[\tilde{\boldsymbol{g}}\left(\boldsymbol{x}|\boldsymbol{\Theta}_f^*\right)-\boldsymbol{g}(\boldsymbol{x})\right]u_* \tag{40}$$

In order to analyze the stability and robustness of the system, the Lyapunov design scheme employed considering the following Lyapunov function candidate

$$\begin{aligned}V(t)=&\frac{1}{2}\boldsymbol{e}^T\boldsymbol{P}\boldsymbol{e}+\frac{1}{2\gamma_f}\left(\boldsymbol{\Theta}_f-\boldsymbol{\Theta}_f^*\right)^T\left(\boldsymbol{\Theta}_f-\boldsymbol{\Theta}_f^*\right)\\&+\frac{1}{2\gamma_g}\left(\boldsymbol{\Theta}_g-\boldsymbol{\Theta}_g^*\right)^T\left(\boldsymbol{\Theta}_g-\boldsymbol{\Theta}_g^*\right)\end{aligned} \tag{41}$$

$$\boldsymbol{\Lambda}^T\boldsymbol{P}+\boldsymbol{P}\boldsymbol{\Lambda}=-\boldsymbol{Q} \tag{42}$$

where $\boldsymbol{P}$ and $\boldsymbol{Q}$ are $n\times n$ are positive definite symmetric and arbitrary positive definite matrices, respectively to satisfy the Lyapunov stability. Considering (40), the tracking error dynamics can be presented as following where the optimal approximation error is also included:

$$\begin{aligned}\dot{\boldsymbol{e}}=&\boldsymbol{\Lambda}\boldsymbol{e}+\boldsymbol{b}\left[\tilde{\boldsymbol{f}}\left(\boldsymbol{x}|\boldsymbol{\Theta}_f\right)-\tilde{\boldsymbol{f}}\left(\boldsymbol{x}|\boldsymbol{\Theta}_f^*\right)\right]+\left[\tilde{\boldsymbol{g}}\left(\boldsymbol{x}|\boldsymbol{\Theta}_f\right)\right.\\&\left.-\tilde{\boldsymbol{g}}\left(\boldsymbol{x}|\boldsymbol{\Theta}_f^*\right)\right]u_*+\tilde{\boldsymbol{w}}\end{aligned} \tag{43}$$

$$\dot{\boldsymbol{e}}=\boldsymbol{\Lambda}\boldsymbol{e}+\boldsymbol{b}\left[\left(\boldsymbol{\Theta}_f-\boldsymbol{\Theta}_f^*\right)^T\boldsymbol{\xi}_f+\left(\boldsymbol{\Theta}_g-\boldsymbol{\Theta}_g^*\right)^T\boldsymbol{\xi}_g u_*+\tilde{\boldsymbol{w}}\right] \tag{44}$$

The time derivative of (41) $\dot{V}$ is obtained as

$$\begin{aligned}\dot{V}(t)=&-\frac{1}{2}\boldsymbol{e}^T\boldsymbol{Q}\boldsymbol{e}+\boldsymbol{e}^T\boldsymbol{Q}\boldsymbol{b}\boldsymbol{w}+\frac{1}{\gamma_f}\left(\boldsymbol{\Theta}_f-\boldsymbol{\Theta}_f^*\right)^T\\&\times\left[\dot{\boldsymbol{\Theta}}_f+\gamma_f\boldsymbol{e}^T\boldsymbol{P}\boldsymbol{b}\boldsymbol{\xi}_f(\boldsymbol{x})\right]+\frac{1}{\gamma_g}\left(\boldsymbol{\Theta}_g-\boldsymbol{\Theta}_g^*\right)^T\\&\times\left[\dot{\boldsymbol{\Theta}}_g+\gamma_g\boldsymbol{e}^T\boldsymbol{P}\boldsymbol{b}\boldsymbol{\xi}_g(\boldsymbol{x})u_*\right]\end{aligned} \tag{45}$$

By considering the terms $\dot{\boldsymbol{\Theta}}_f+\gamma_f\boldsymbol{e}^T\boldsymbol{P}\boldsymbol{b}\boldsymbol{\xi}_f(\boldsymbol{x})$ and $\dot{\boldsymbol{\Theta}}_g+\gamma_g\boldsymbol{e}^T\boldsymbol{P}\boldsymbol{b}\boldsymbol{\xi}_g(\boldsymbol{x})u_*$ at zero, the adaptation laws of $\boldsymbol{\Theta}_f$ and $\boldsymbol{\Theta}_g$, can be obtained as follows:

$$\begin{aligned}\dot{\boldsymbol{\Theta}}_f &\triangleq -\gamma_f\boldsymbol{e}^T\boldsymbol{P}\boldsymbol{b}\boldsymbol{\xi}_f(\boldsymbol{x})\\ \dot{\boldsymbol{\Theta}}_g &\triangleq -\gamma_g\boldsymbol{e}^T\boldsymbol{P}\boldsymbol{b}\boldsymbol{\xi}_g(\boldsymbol{x})u_*\end{aligned} \tag{46}$$

where the $\boldsymbol{e^TPb}$ term is scalar and by considering the eigenvalues of arbitrary positive definite matrix Q sufficiently large, once can and small approximation error w (convergence to the ideal parameters by employing updated stochastic gradient descent based NN approximator), one can write:

$$\dot{V}(t)\le-\frac{1}{2}\boldsymbol{e}^T\boldsymbol{Q}\boldsymbol{e}+\boldsymbol{e}^T\boldsymbol{Q}\boldsymbol{b}\boldsymbol{w}\le 0 \tag{47}$$

Barbalat's lemma is used to indicate that $\lim_{t\to\infty}\mathrm{e}=0$, it has to be shown that $\boldsymbol{e}\in L_2$ and $\dot{\boldsymbol{e}}$ is bounded, such that the term in (45) can be described as:

$$\int_0\dot{V}(\tau)\,d\tau=V(t)-V(0) \tag{48}$$

Considering (41) which is a positive definite and non-increasing term therefore (48) can be stated as:

$$\begin{aligned}\int_0\dot{V}(\tau)\,d\tau=V(t)-V(0)&\xrightarrow{\times(-1)}-\int_0\dot{V}(\tau)\,d\tau\\&=V(0)-V(t)<\infty\end{aligned} \tag{49}$$

Also by considerin $\hat{\lambda}$ as the maximum eigenvalue of $\boldsymbol{Q}$ in (36), and taking (41) into account, it can be shown that

$$\frac{1}{2}\boldsymbol{e}^T\boldsymbol{Q}\boldsymbol{e} \leq \frac{1}{2}\hat{\lambda}\left\|\boldsymbol{e}\right\|^2 \tag{50}$$

Taking (43) into account, such that

$$\int_0^t \frac{1}{2}\hat{\lambda}\left\|\boldsymbol{e}\right\|^2 d\tau < \infty \tag{51}$$

And therefore:

$$\int_0^t \frac{1}{2}\hat{\lambda}\left\|\boldsymbol{e}\right\|^2 d\tau^{1/2} < \infty \tag{52}$$

That shows $\boldsymbol{e} \in l^2$ which implies that $\dot{\boldsymbol{e}} \in L_\infty$, and thereby the asymptotic convergence of the tracking error $\boldsymbol{e}$ is derived using the Barbala's lemma

$$\lim_{t\to\infty} |e| = 0 \tag{53}$$

This completes the proof of proposed controller stability ■.

The closed-loop system is robust globally asymptotically stable. Additionally, the parameters defined in (33) are in terms of the non-ideal terms (*i.e.* $\boldsymbol{x}|\boldsymbol{\Theta}_{f,g}$) and thereby the approximation error term in (40) can be increased while its minimization can further contribute to the asymptotic stability in (45). Therefore, a NN based approximator with employing an updated stochastic gradient descent method is proposed to obtain the ideal function parameters (*i.e.* $\boldsymbol{x}|\boldsymbol{\Theta}^*_{f,g}$). Furthermore, the approximation errors of $\boldsymbol{E_f}$ and $\boldsymbol{E_g}$ are defined as

$$\begin{aligned} \boldsymbol{e_f} &\triangleq \tilde{\boldsymbol{f}}\left(\boldsymbol{x}|\boldsymbol{\Theta}^*_f\right) - \tilde{\boldsymbol{f}}\left(\boldsymbol{x}|\boldsymbol{\Theta}_f\right) \\ \boldsymbol{e_g} &\triangleq \tilde{\boldsymbol{g}}\left(\boldsymbol{x}|\boldsymbol{\Theta}^*_g\right) - \tilde{\boldsymbol{f}}\left(\boldsymbol{x}|\boldsymbol{\Theta}_g\right) \end{aligned} \tag{54}$$

And because is assumed that $\boldsymbol{f}(\boldsymbol{x})$ and $\boldsymbol{g}(\boldsymbol{x})$ are bounded functions, and thereby $\boldsymbol{e}_f$ and $\boldsymbol{e}_g$ in (54) are bounded and the term $\boldsymbol{E}$ to be minimized can be considered as:

$$\boldsymbol{E}_{f,g}(t) = \frac{1}{2}\left(\boldsymbol{e}_{f,g}\right)^2 \tag{55}$$

Using the gradient descent optimization method, the updated error to be minimized can be presented in the general form as

$$\begin{aligned} \boldsymbol{\Theta}^*_f(t+1) &= \boldsymbol{\Theta}^*_f(t) - \eta\frac{\partial \boldsymbol{E}_f(t)}{\partial \boldsymbol{\Theta}^*_f(t)} \\ \boldsymbol{\Theta}^*_g(t+1) &= \boldsymbol{\Theta}^*_g(t) - \eta\frac{\partial \boldsymbol{E}_g(t)}{\partial \boldsymbol{\Theta}^*_g(t)} \end{aligned} \tag{56}$$

Using the chain rule, the above equation can be written as:

$$\begin{aligned} \boldsymbol{\Theta}^*_f(t+1) &= \boldsymbol{\Theta}^*_f(t) - \eta\frac{\partial \boldsymbol{E}_f(t)}{\partial \boldsymbol{e}(t)}\frac{\partial \boldsymbol{e}(t)}{\partial \boldsymbol{x}(t)}\frac{\partial \boldsymbol{x}(t)}{\partial \tilde{\boldsymbol{f}}(t)}\frac{\partial \tilde{\boldsymbol{f}}(t)}{\partial \boldsymbol{\Theta}^*_f(t)} \\ \boldsymbol{\Theta}^*_g(t+1) &= \boldsymbol{\Theta}^*_g(t) - \eta\frac{\partial \boldsymbol{E}_g(t)}{\partial \boldsymbol{e}(t)}\frac{\partial \boldsymbol{e}(t)}{\partial \boldsymbol{x}(t)}\frac{\partial \boldsymbol{x}(t)}{\partial \tilde{\boldsymbol{g}}(t)}\frac{\partial \tilde{\boldsymbol{g}}(t)}{\partial \boldsymbol{\Theta}^*_g(t)} \end{aligned} \tag{57}$$

The minimum of the error functions are reduced based on the obtained first-order iterative method and the step size term η is allowed to change iteratively. Considering the minimization functions $\boldsymbol{E}_{f,g}$ being convex and $\partial\boldsymbol{E}_{f,g}$ Lipschitz and selection of η through the (51), the convergence to the minimum is updated and ensured considering the learning rate as follows.

$$\eta(t) = \frac{\left(\boldsymbol{\theta}_f(t) - \boldsymbol{\theta}_f(t-1)\right)^T\left[\boldsymbol{E}_f(t) - \boldsymbol{E}_f(t-1)\right]}{\left\|\boldsymbol{E}_f(t) - \boldsymbol{E}_f(t-1)\right\|^2} \tag{58}$$

In order to decrease the monotonic decrement of the step size term, the accumulated previous squared gradients are condensed into a certain window Ψ where the sum of gradients is iteratively described through exponentially decaying average of the squared gradients. For brevity, let us consider the gradient of the objective function as follows:

$$\frac{\partial \boldsymbol{E}_{f,g}(t)}{\partial \boldsymbol{\theta}_{f,g}(t)} = \nabla_\theta \beth(\theta) \tag{59}$$

Considering the running average at time t is denoted by $E[(\nabla_\theta \beth(\theta))^2]_t$ which can be calculated as [36]:

$$E[(\nabla_\theta \beth(\boldsymbol{\theta}))^2]_t = \Phi E[(\nabla_\theta \beth(\boldsymbol{\theta}))^2]_{t-1} + (1-\Phi)\left(\nabla_\theta \beth(\boldsymbol{\theta})\right)^2_t \tag{60}$$

where Φ represents the decaying variable in analogy with the Momentum approach and it can be perceived that at any increased step, the above running mean is a function of the former average of squared gradients and the present squared gradients. Assuming that the stochastic gradient descent of updates is represented by

$$\boldsymbol{\theta}_{f,g}(t+1) = \boldsymbol{\theta}_{f,g}(t) - \eta\nabla_\theta \beth(\boldsymbol{\theta}) \tag{61}$$

The vectorized parameter updates can be performed based on previous gradients as in [23], [36], [37] throughout the following

$$\begin{aligned} \Delta\boldsymbol{\theta}_t &= \boldsymbol{\theta}_{f,g}(t+1) - \boldsymbol{\theta}_{f,g}(t) \\ &= -\frac{\eta}{\sqrt{G_t + \epsilon}} \odot \nabla_{\boldsymbol{\theta}} \beth(\boldsymbol{\theta}) \end{aligned} \tag{62}$$

where $\odot$ is the matrix-vector operator, and G_t is a diagonal matrix which involves the sum of the squares of the previous gradients, and small constant ϵ is included to ensure the denominator does not converge to zero. Because the term in (60) is presented through the average of squared gradients, the root means square (RMS) of previous squared gradients is calculated as [34]:

$$RMS\left[\Delta\boldsymbol{\theta}\right]_t = \left(\Delta\boldsymbol{\theta}_t + \epsilon\right)^{0.5} \tag{63}$$

It is noteworthy that the diagonal matrix can be substituted by decaying average across previous gradients $E[(\nabla_\theta \beth(\theta))^2]_t$. The computed updates can be shown as

$$\Delta\boldsymbol{\theta}_t = -\frac{\eta}{RMS\left[\Delta\boldsymbol{\theta}\right]_t}\nabla_{\boldsymbol{\theta}} \beth(\boldsymbol{\theta}) \tag{64}$$

However, the output in (61) is unidentified and thereby, (62) can be calculated by employing the exponentially decaying of (61) across a window Ψ instead of the learning rate

obtained in the previously step which finally can be presented as:

$$\boldsymbol{\Theta}_f^*(t+1) = \boldsymbol{\Theta}_f^*(t) - \frac{RMS\,[\Delta\boldsymbol{\theta}]_{t-1}}{RMS\,[\Delta\theta]_t} \frac{\partial \boldsymbol{E_f}(t)}{\partial \boldsymbol{e}(t)} \frac{\partial \boldsymbol{e}(t)}{\partial \boldsymbol{x}(t)} \frac{\partial \boldsymbol{x}(t)}{\partial \tilde{\boldsymbol{f}}(t)} \times \frac{\partial \tilde{\boldsymbol{f}}(t)}{\partial \boldsymbol{\Theta}_f^*(t)}$$

$$\boldsymbol{\Theta}_g^*(t+1) = \boldsymbol{\Theta}_g^*(t) - \frac{RMS\,[\Delta\boldsymbol{\theta}]_{t-1}}{RMS\,[\Delta\boldsymbol{\theta}]_t} \frac{\partial \boldsymbol{E_g}(t)}{\partial \boldsymbol{e}(t)} \frac{\partial \boldsymbol{e}(t)}{\partial \boldsymbol{x}(t)} \frac{\partial \boldsymbol{x}(t)}{\partial \tilde{\boldsymbol{g}}(t)} \times \frac{\partial \tilde{\boldsymbol{g}}(t)}{\partial \boldsymbol{\Theta}_g^*(t)} \quad (65)$$

V. RESULTS AND DISCUSSIONS

The objectives as mentioned are defined in (11) in terms of the attenuation of the seat acceleration which is closely associated with the force exerted to the driver at the seat interface, also the head acceleration which is also very significant for the comfort experience of the driver and the relative displacement between the cabin floor and the seat. For this purpose, the commercial vehicle cabin excitation (EM5) based on ISO 7096 related to an extensive range of commercial vehicles such as soil compactor, wheel dozer, and Backhoe loader is employed. The high-pass and low-pass filters of Butterworth type are designated. The low-pass filter and high-pass filters are 6 and 24 decibels per octave and their corresponding cut-off frequencies are 3.5 and 1.5 Hz, respectively. Moreover, the maximum PSD of vertical vibration at the platform is 0.77 $[(m/s^2)^2/Hz]$. The total weighting function employed is a combination of I) band-limiting two-pole filter with Butterworth characteristics, *II*) acceleration-velocity transition which is proportionality to acceleration at lower frequencies with proportionality to the velocity at higher frequencies) and *III*) Upward step which is steepness approximately 6 dB per octave and proportionality to jerk. The PSD of cabin excitations for a typical commercial vehicle generated in accordance with the ISO 7096 is illustrated in Fig. 4. In the initial stage, a total of 11 uniformly random numbers between 0 and 1 were employed for the upper and lower MFs, respectively, and γ_f and γ_g equal to 0.4 were employed. The weighted seat accelerations and PSD of seat accelerations for the passive system obtained from a high-fidelity validation platform using MSC ADAMS, an observer-based sliding mode controller (DO-SMC) from the literature [19] and T2FNN-adaptive stochastic gradient descent (SGD) controller is illustrated in Fig. 5. It can be seen that the weighted seat accelerations based on ISO 2631 have been decreased using the DO-SMC during the entire range of the simulation, however, the T2FNN-adaptive SGD has exhibited a significantly improved performance against the cabin excitations as the external disturbance. The RMS values of weighted accelerations were obtained at 3.8, 2.7, and 0.78 m/s^2 for the uncontrolled, DO-SMC and the proposed controller, respectively. Fig. 5 also illustrates the PSD of accelerations in frequency domain for the same controller strategies. It can be appreciated that the proposed T2FNN-adaptive SGD presents significantly improved vibration attenuation when compared to the passive and DO-SMC over the entire frequency range and particularly between the range of 4-6 Hz which is more important from the biodynamic point of view where the primary resonance frequency of the human body is included. The peak PSD magnitudes of the accelerations are 18.34, 8.01 and 0.25 m^2/s^3 for the same control strategies, respectively (Fig. 5).

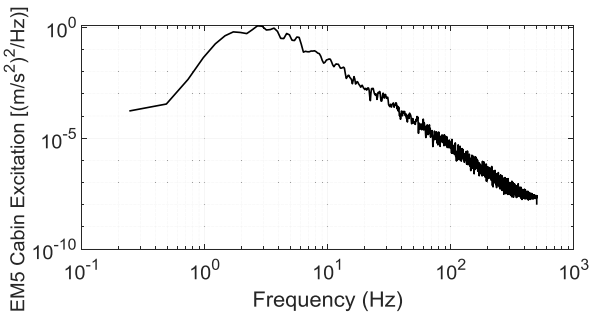

FIGURE 4. PSD of cabin excitations (EM5) with respect to the frequency based on ISO 7096.

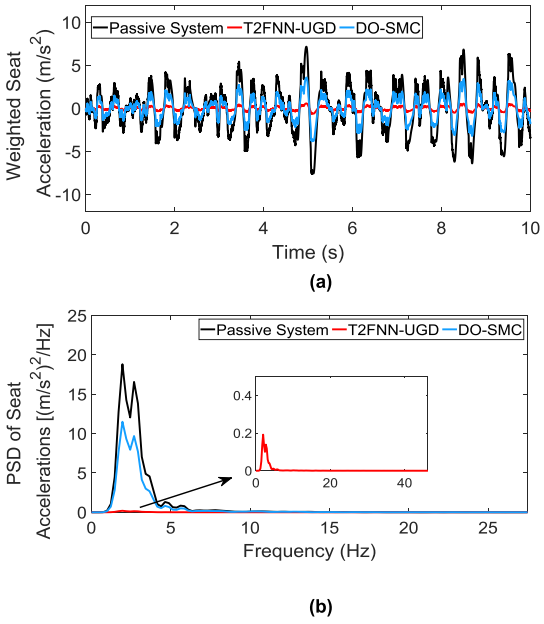

FIGURE 5. a) The weighted seat accelerations and b) PSD of seat accelerations for the uncontrolled, DO-SMC [19] and T2FNN-adaptive stochastic GD controller.

Figure 6 illustrates the time-history relative displacement between the seat and the cabin floor as well as the frequency domain responses. The obtained results show that the RMS of the relative displacements is in the order of 0.08, 0.032, and 0.028 m, for the DO-SMC, proposed method and the passive system. It was expectable that while the focus is on reducing the seat accelerations, the relative displacement has to be inherently increased, however, the proposed method has maintained the relative displacement close to the passive system so that the risk of collision with the seat endstops are decreased. The maximum PSD of the relative displacements are suggestive of 0.0004, 0.0001 and 0.0002 m^2 at the

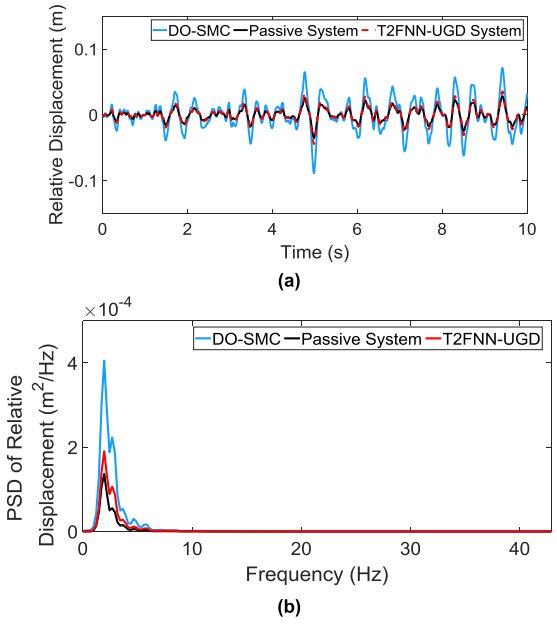

FIGURE 6. a) The relative displacement and b) PSD of relative displacement for the uncontrolled, DO-SMC [19] and T2FNN-adaptive stochastic GD controller.

resonance frequency of 1.9 Hz for the DO-SMC, the proposed controller and the passive system, respectively. It can be seen that the relative displacement which is closely related to the relative motion of the legs with respect to the cabin floor has not been much increased when employing DO-SMC. The proposed controller however, has maintained the system close to the optimal relative displacement which is perhaps related to the gradient descent method employed which provides an enhanced convergence to a minimum error via the adaptive time-step based gradient method being employed. It supplies better performance for a fast and accurate convergence with minimal chance of being entrapped in a saddle point, which increases the optimization performance of the controller and thereby an optimal solution to minimize the tracking error.

The head acceleration is an important body segment and affects the ride experience and directly affects the driver in prolonged work time and based on 8-hour standard. The performance of the proposed controller against the uncontrolled system and DO-SMC can be seen in Fig. 7. It can be seen that similar to the weighted seat accelerations, the accelerations transmitted through the body segments and from the cabin floor to the head according to (4) and (6), the proposed controller offers a minimized acceleration transmission to the head in the both of frequency and time domains. The derived RMS of weighted accelerations for the uncontrolled, DO-SMC and the proposed controller are 3.94, 2.1, and 0.25 m/s^2, respectively, which is suggestive of the improved performance of the proposed controller. As for the frequency domain, the peak values are those obtained at 2.68 Hz equal to 3.6, 0.81 and 0.02 m^2/s^3, respectively, for the uncontrolled, DO-SMC and the proposed controller. Fig. 7 also demonstrates the frequency response of the acceleration in terms of the number of peaks related to the degree-of-freedom

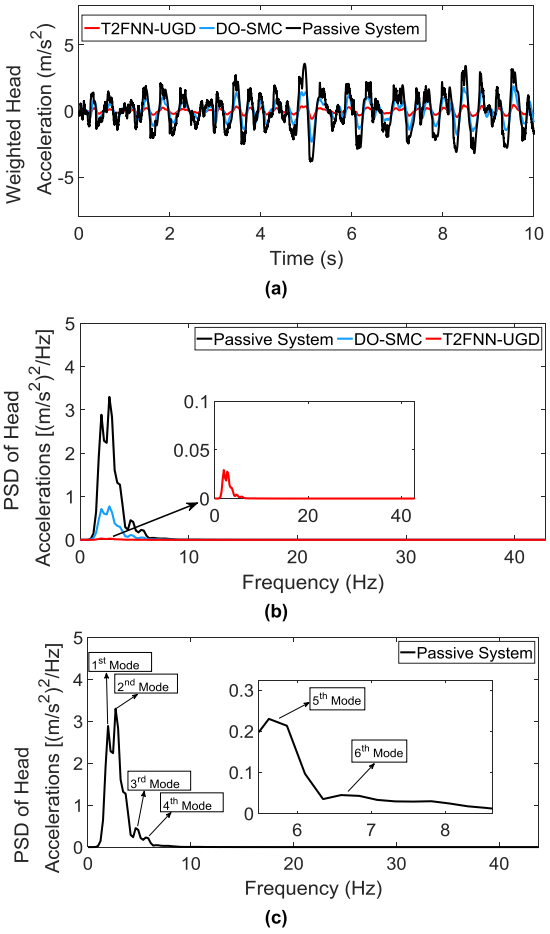

FIGURE 7. a) The weighted head accelerations, b) PSD of head accelerations for the uncontrolled, DO-SMC [19] and T2FNN-adaptive stochastic GD controller, and c) the PSD of acceleration in the frequency domain including the 6 uncoupled modes of vibration.

(6-DOFs). It is evident that the peaks depend on the excitation spectrum of the frequency components. Finally, the control effort for the proposed controller can be seen in Fig. 8, where the peak value is obtained at the beginning equal to 1106 N but due to the adaptive stochastic gradient descent learning rate, it converged quickly to the intimal value. The RMS of the control effort was also achieved at 152.5 N and the noisy signal of the control input is more likely related to the scholastic gradient descent optimization method being employed. The obtained results compared to [19] are suggestive of more promising control results. Although the nonlinear seat suspension is considered in the present study and the PSD of accelerations are invariably greater compared to [19], however, the obtained head and body acceleration in the present study are smaller. Furthermore, the challenging demand for an increased relative displacement by decreasing body acceleration is not considered in [19]. Finally, due to applying SMC method for the controller, the control input has a high-frequency component as a result of chattering phenomenon while the proposed controller in this paper generates a reasonably acceptable signal (Fig. 8) in a smaller power demand than DO-SMC [19]. Finally,

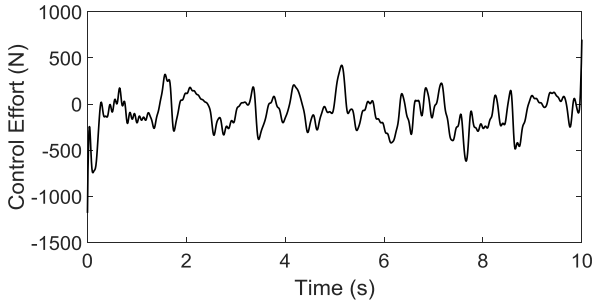

FIGURE 8. The control effort of the proposed adaptive-T2FNN based stochastic GD controller.

in order to investigate the effectiveness of the proposed controller to withstand the effect of parametric uncertainties, masses, stiffness and damping values varied $\pm 15\%$ about the nominal values such that $\{m_i = m_i + 0.15m_i \sin(t)$, $c_j = c_j + 0.15c_j \sin(t)$ & $k_j = k_j + 0.15k_j \sin(t)$; $i = 1, 2, ..6$ & $j = 1, 2, ..5\}$. The results are presented in Table 2, where it is evident that the proposed controller can decrease the magnitude of the transmitted acceleration to head when compared to DO-SMC and the passive system while there are variations of the mechanical components of the system at varied $\pm 15\%$ about the nominal values.

TABLE 2. RMS of head acceleration (m/s^2) under the effect of parametric uncertainty.

Controller type	Without uncertainty (m/s^2)	With Uncertainty (m/s^2)
Passive System	3.94	4.23
Proposed Control	0.25	0.67
DO-SMC [19]	2.11	2.83

VI. CONCLUSIONS

In this paper, an adaptive indirect type-2 fuzzy neural network optimized through an adaptive stochastic gradient descent algorithm was proposed as a robust controlling schema to deal with the attenuation of seated whole-body vibration in typical commercial vehicles. The cabin excitations were in accordance with the ISO 7096 where the high-pass and low-pass filters of the Butterworth type were designated and the weighted accelerations of the human body segments were evaluated based on ISO 2631. To this end, a 6-DOF coupled human-body and seat suspension system model was developed. The objectives were the minimization of the accelerations transferred to the head and at the seat which are closely relate to the safety and ride smoothness of the driver, particularly in the prolonged working conditions, and the relative seat and cabin floor displacement which is related to the relative motion of the legs with respect to the tights and pelvis. In the controller section, a T2FNN controller was designed and to guarantee the closed-loop system stability and also to derive the adaptation laws, the Lyapunov stability method was used. The interval type-2 fuzzy Gaussian membership function with uncertain standard deviations were used in the study and the optimal parameters of the mean and standard deviations are adjusted through an updated gradient descent optimization method. An adaptive stochastic gradient descent based optimization coupled to the T2FNN was developed in order to reach an improved performance of the controller. The results compared to the uncontrolled system and DO-SMC schema both in time domain and frequency domain (in terms of the RMS and PSD of the weighted accelerations) confirmed that the proposed controller can drastically reduce the objective head and seat accelerations and significantly reduce the relative seat to cabin displacement owing to the proposed adaptive stochastic gradient descent method. Future studies can be implemented related to the computational demand and the actuation time delay for these controllers in a comparative trend.

REFERENCES

[1] S.-B. Choi and Y.-M. Han, "Vibration control of electrorheological seat suspension with human-body model using sliding mode control," *J. Sound Vibrat.*, vol. 303, nos. 1–2, pp. 391–404, Jun. 2007.
[2] H. Taghavifar and A. Mardani, "Off-road vehicle dynamics," in *Off-road Vehicle Dynamics: Analysis, Modelling and Optimization* (Studies in Systems, Decision and Control), vol. 70. Cham, Switzerland: 2017, p. 37.
[3] H. Taghavifar and S. Rakheja, "Multi-objective optimal robust seat suspension control of off-road vehicles in the presence of disturbance and parametric uncertainty using metaheuristics," *IEEE Trans. Intell. Vehicles*, early accesss, Dec. 23, 2019, doi: 10.1109/TIV.2019.2960927.
[4] H. Taghavifar and S. Rakheja, "Parametric analysis of the potential of energy harvesting from commercial vehicle suspension system," *Proc. Inst. Mech. Eng., Part D, J. Automobile Eng.*, vol. 233, no. 11, pp. 2687–2700, Sep. 2019.
[5] H. Taghavifar and S. Rakheja, "Supervised ANN-assisted modeling of seated body apparent mass under vertical whole body vibration," *Measurement*, vol. 127, pp. 78–88, Oct. 2018.
[6] Z. Zhou and M. J. Griffin, "Response of the seated human body to whole-body vertical vibration: Biodynamic responses to sinusoidal and random vibration," *Ergonomics*, vol. 57, no. 5, pp. 693–713, May 2014.
[7] J. L. Coyte, D. Stirling, H. Du, and M. Ros, "Seated whole-body vibration analysis, technologies, and modeling: A survey," *IEEE Trans. Syst., Man, Cybern. Syst.*, vol. 46, no. 6, pp. 725–739, Jun. 2016.
[8] C.-C. Liang and C.-F. Chiang, "Modeling of a seated human body exposed to vertical vibrations in various automotive postures," *Ind. Health*, vol. 46, no. 2, pp. 125–137, 2008.
[9] H. Taghavifar, "Reduced vibration of off-road vehicle nonlinear suspension system using an adaptive integral sliding mode-neural network controller," *Int. J. Dyn. Control*, vol. 8, no. 1, pp. 291–301, Mar. 2020.
[10] M. Gudarzi and A. Oveisi, "Robust control for ride comfort improvement of an active suspension system considering uncertain driver's biodynamics," *J. Low Freq. Noise, Vibrat. Act. Control*, vol. 33, no. 3, pp. 317–339, Sep. 2014.
[11] Z. Gu, S. Fei, Y. Zhao, and E. Tian, "Robust control of automotive active seat-suspension system subject to actuator saturation," *J. Dyn. Syst., Meas., Control*, vol. 136, no. 4, pp. 1–7, Jul. 2014.
[12] M. Lathkar, A. Tiwari, P. D. Shendge, and S. B. Phadke, "Active seat suspension based on second order inertial delay control combined with sliding mode control," in *Proc. IEEE 1st Int. Conf. Power Electron., Intell. Control Energy Syst. (ICPEICES)*, Jul. 2016, pp. 1–5.
[13] S. Wen, M. Z. Q. Chen, Z. Zeng, X. Yu, and T. Huang, "Fuzzy control for uncertain vehicle active suspension systems via dynamic sliding-mode approach," *IEEE Trans. Syst., Man, Cybern. Syst.*, vol. 47, no. 1, pp. 24–32, Jan. 2017.
[14] D. Ning, S. Sun, F. Zhang, H. Du, W. Li, and B. Zhang, "Disturbance observer based Takagi-PSugeno fuzzy control for an active seat suspension," *Mech. Syst. Signal Process.*, vol. 93, pp. 515–530, Sep. 2017.
[15] R. Guclu, "Fuzzy logic control of seat vibrations of a non-linear full vehicle model," *Nonlinear Dyn.*, vol. 40, no. 1, pp. 21–34, Apr. 2005.
[16] Y. Qin, X. Tang, T. Jia, Z. Duan, J. Zhang, Y. Li, and L. Zheng, "Noise and vibration suppression in hybrid electric vehicles: State of the art and challenges," *Renew. Sustain. Energy Rev.*, vol. 124, May 2020, Art. no. 109782.

[17] C. Hu, Z. Wang, H. Taghavifar, J. Na, Y. Qin, J. Guo, and C. Wei, "MME-EKF-based path-tracking control of autonomous vehicles considering input saturation," *IEEE Trans. Veh. Technol.*, vol. 68, no. 6, pp. 5246–5259, Jun. 2019.
[18] H. Du, W. Li, and N. Zhang, "Integrated seat and suspension control for a quarter car with driver model," *IEEE Trans. Veh. Technol.*, vol. 61, no. 9, pp. 3893–3908, Nov. 2012.
[19] M. S. Lathkar, P. D. Shendge, and S. B. Phadke, "Active control of uncertain seat suspension system based on a state and disturbance observer," *IEEE Trans. Syst., Man, Cybern., Syst.*, vol. 50, no. 3, pp. 840–850, Mar. 2020.
[20] D. Ning, S. Sun, L. Wei, B. Zhang, H. Du, and W. Li, "Vibration reduction of seat suspension using observer based terminal sliding mode control with acceleration data fusion," *Mechatronics*, vol. 44, pp. 71–83, Jun. 2017.
[21] S. A. Chen, J. C. Wang, M. Yao, and Y. B. Kim, "Improved optimal sliding mode control for a non-linear vehicle active suspension system," *J. Sound Vibrat.*, vol. 395, pp. 1–25, Mar. 2017.
[22] D. Ning, H. Du, S. Sun, W. Li, and B. Zhang, "An innovative two-layer multiple-DOF seat suspension for vehicle whole body vibration control," *IEEE/ASME Trans. Mechatronics*, vol. 23, no. 4, pp. 1787–1799, Aug. 2018.
[23] C. Hu, H. Gao, J. Guo, H. Taghavifar, Y. Qin, J. Na, and C. Wei, "RISE-based integrated motion control of autonomous ground vehicles with asymptotic prescribed performance," *IEEE Trans. Syst., Man, Cybern. Syst.*, early access, Nov. 12, 2019, doi: 10.1109/TSMC.2019.2950468.
[24] H. Taghavifar, A. M. Motlagh, A. Mardani, A. Hassanpour, A. H. Hosseinloo, L. Taghavifar, and C. Wei, "Appraisal of Takagi–Sugeno type neuro-fuzzy network system with a modified differential evolution method to predict nonlinear wheel dynamics caused by road irregularities," *Transport*, vol. 31, no. 2, pp. 211–220, Jun. 2016.
[25] Q. Zhou, P. Shi, S. Xu, and H. Li, "Adaptive output feedback control for nonlinear time-delay systems by fuzzy approximation approach," *IEEE Trans. Fuzzy Syst.*, vol. 21, no. 2, pp. 301–313, Apr. 2013.
[26] Q. Zhou, P. Shi, J. Lu, and S. Xu, "Adaptive output-feedback fuzzy tracking control for a class of nonlinear systems," *IEEE Trans. Fuzzy Syst.*, vol. 19, no. 5, pp. 972–982, Oct. 2011.
[27] A. Mohammadzadeh, O. Kaynak, and M. Teshnehlab, "Two-mode indirect adaptive control approach for the synchronization of uncertain chaotic systems by the use of a hierarchical interval type-2 fuzzy neural network," *IEEE Trans. Fuzzy Syst.*, vol. 22, no. 5, pp. 1301–1312, Oct. 2014.
[28] M. A. Khanesar, E. Kayacan, M. Teshnehlab, and O. Kaynak, "Analysis of the noise reduction property of type-2 fuzzy logic systems using a novel type-2 membership function," *IEEE Trans. Syst., Man, Cybern. B. Cybern.*, vol. 41, no. 5, pp. 1395–1406, Oct. 2011.
[29] H. Taghavifar and S. Rakheja, "Path-tracking of autonomous vehicles using a novel adaptive robust exponential-like-sliding-mode fuzzy type-2 neural network controller," *Mech. Syst. Signal Process.*, vol. 130, pp. 41–55, Sep. 2019.
[30] M. M. Zirkohi and T.-C. Lin, "Interval type-2 fuzzy-neural network indirect adaptive sliding mode control for an active suspension system," *Nonlinear Dyn.*, vol. 79, no. 1, pp. 513–526, Jan. 2015.
[31] *Earth-Moving Machinery—Laboratory Evaluation of Operator Seat Vibration*, Standard EN ISO 7096, Eur. Committee Standardization, Brussels, Belgium 2000.
[32] *Mechanical vibration and Shock-Evaluation of Human Exposure to Whole-Body Vibration. Part1: General Requirements*, Standard ISO. 2631-1, 1997.
[33] P.-É. Boileau and S. Rakheja, "Whole-body vertical biodynamic response characteristics of the seated vehicle driver: Measurement and model development," *Int. J. Ind. Ergonom.*, vol. 22, no. 6, pp. 449–472, Dec. 1998.
[34] A. Mohammadzadeh and S. Ghaemi, "A modified sliding mode approach for synchronization of fractional-order chaotic/hyperchaotic systems by using new self-structuring hierarchical type-2 fuzzy neural network," *Neurocomputing*, vol. 191, pp. 200–213, May 2016.
[35] N. N. Karnik, J. M. Mendel, and Q. Liang, "Type-2 fuzzy logic systems," *IEEE Trans. Fuzzy Syst.*, vol. 7, no. 6, pp. 643–658, Dec. 1999.
[36] S. Ruder, "An overview of gradient descent optimization algorithms," 2016, *arXiv:1609.04747*. [Online]. Available: http://arxiv.org/abs/1609.04747
[37] M. D. Zeiler, "ADADELTA: An adaptive learning rate method," 2012, *arXiv:1212.5701*. [Online]. Available: http://arxiv.org/abs/1212.5701

HAMID TAGHAVIFAR (Member, IEEE) received the Ph.D. degree in mechanical engineering from Urmia University, Iran, in 2016. He is currently an Assistant Professor with the School of Mechanical, Aerospace and Automotive Engineering, Coventry University, U.K. Previously, he was a Horizon Postdoctoral Fellow at the Department of Mechanical, Industrial and Aerospace Engineering, CONCAVE Research Center, Concordia University, Canada. His research interests include vehicle dynamics and control, terramechanics and mechatronics, adaptive and nonlinear controls, artificial intelligence, and optimizations, where he has contributed over 45 articles, a book, and holds two Iranian registered patents. He serves as the Editor-in-Chief of *Journal of Advances in Vehicle Engineering* and an Editor of *International Journal of Vehicle Systems Modelling and Testing* and *International Journal of Vehicle Information and Communication Systems*.

BIN XU received the B.Sc. and Ph.D. degrees in mechanical engineering from the Beijing Institute of Technology, China, in 2005 and 2013, respectively. He is currently an Associate Professor with the Vehicle Research Center, Beijing Institute of Technology. His research interests include aerial and ground vehicle and its dynamic control.

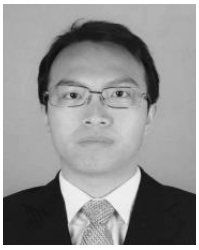

CHUAN HU (Member, IEEE) received the B.E. degree in vehicle engineering from Tsinghua University, Beijing, China, in 2010, the M.E. degree in vehicle operation engineering from the China Academy of Railway Sciences, Beijing, in 2013, and the Ph.D. degree in mechanical engineering from McMaster University, Hamilton, Canada, in 2017. He is currently a Postdoctoral Fellow at the Department of Systems Design Engineering, University of Waterloo, Waterloo, Canada. His research interests include vehicle system dynamics and control, motion control and estimation of autonomous vehicles, mechatronics, and robust and adaptive control.

YECHEN QIN (Member, IEEE) received the B.Sc. and Ph.D. degrees in mechanical engineering from the Beijing Institute of Technology, Beijing, China, in 2010 and 2016, respectively. From 2013 to 2014, he was a Visiting Ph.D. Student with Texas A&M University, College Station, TX, USA. He was also a Postdoctoral Research Fellow and a Visiting Scholar with the Beijing Institute of Technology and the University of Waterloo, Waterloo, ON, Canada. He is currently an Associate Professor with the Beijing Institute of Technology. His current research interests include vehicle dynamics control and road estimation.

CHONGFENG WEI (Member, IEEE) received the B.Sc. degree in computational and applied mathematics and the M.Sc. degree in vehicle engineering from Southwest Jiaotong University, Chengdu, China, in 2009 and 2011, respectively, and the Ph.D. degree in mechanical engineering from the University of Birmingham, in 2015. After two and a half years postdoctoral research period, he joined the School of Mechanical Engineering, Shanghai Jiao Tong University, as an Assistant Professor (tenure-track). He then moved to the Institute of Transport Studies, University of Leeds, in 2018, as a Research Fellow. His current research interests include human-like autonomous vehicle control and collision avoidance.